An Ultra-Low-Voltage and Low-Power ×2 Subharmonic Downconverter Mixer

Shan He and Carlos E. Saavedra, *Senior Member, IEEE*

***Abstract*—An 8.6 GHz ×2 subharmonic mixer with complementary current-reuse to enable ultra-low-voltage and low-power operation is presented. The RF transconductance stage of the mixer uses inductive source degeneration and the mixing core uses four transistors that are driven by a quadrature LO signal. A Volterra series analysis is carried out to determine the optimal gate biasing of the transconductor circuit to maximize the third-order intercept point (IIP_3) performance of the RF stage and of the entire mixer. Experimental results show that the mixer has a conversion gain of 6.0 dB and an IIP_3 of −8.0 dBm. The entire circuit draws 0.6 mW from a 0.6 V supply. The chip was fabricated in a standard 130 nm CMOS process.**

***Index Terms*—Complementary current-reuse topology, down conversion mixer, moderate inversion, subharmonic mixer, ultra-low power, ultra-low voltage.**

I. Introduction

IT IS WELL-KNOWN that with smaller feature sizes in CMOS devices there is a corresponding downward scaling in the supply voltage, which is beneficial for designing low-voltage and low-power RFICs. However, this advantage is counterbalanced by the fact that the threshold voltage of the CMOS transistor does not scale down as aggressively as its minimum feature size due to the effect of the subthreshold current leakage [1]. The non-scaling of the threshold voltage reduces the overdrive voltage on the MOSFETs, and it is almost inevitable that the devices have to be operated in the weak to moderate inversion regions [2]. As a result, the linearity performance of low-voltage circuits is diminished and specialized techniques have been developed to bring the linearity back to acceptable levels. Some of those techniques include folded circuit configurations and complementary current-reuse topologies [3]–[6].

In the area of silicon-based active mixers, most of the work on low-power design has focused on fundamental-mode mixers, but there has been some amount of work on subharmonic mixers as well [5]–[10]. It is of interest to further develop low-power subharmonic mixers because these circuits offer design alternatives to radio system engineers, such as the ability to use lower-frequency LO signals with better phase noise performance than high-frequency LO signals. Another important use of subharmonic mixers is in direct-conversion (zero IF) receivers in order to mitigate the deleterious phenomenon known as LO self-mixing, which degrades the baseband information [8], [11].

While the low-power active subharmonic mixers reported to date can operate in the milliwatt range, they have still relied on supply voltages close to or above 1 V. In this paper we present a ×2 subharmonic mixer that is both low-power and low-voltage, drawing only 0.6 mW from a 0.6 V supply. The mixer employs a complementary current-reuse technique and it has an inductive source degenerated RF transconductance stage. The switching core consists of four transistors arranged in pairs of two to carry out both the mixing and LO doubling operations. A Volterra series analysis of the RF transconductance stage is carried out in order to determine the optimal gate biasing to maximize the IIP_3 performance of that stage and, by extension, of the entire mixer. The analysis also reveals that there is a trade-off between the optimal gate biasing and the amount of source degeneration that should be used in the circuit. Measured results show that the mixer has 6.0 dB of conversion gain and an IIP_3 of −8.0 dBm.

II. Ultra-Low-Voltage ×2 Subharmonic Mixer

In this section, a qualitative description of the mixer operation is presented first followed by a detailed investigation of the distortion behavior of the circuit. Specifically, Volterra series analysis is used to examine the effect of inductive source degeneration on the mixer's distortion performance.

A. Overall Circuit Description

Fig. 1 illustrates the proposed single-balanced ×2 subharmonic ultra-low-voltage down-converter mixer. In the RF stage of the mixer, transistor M_1 serves as a transconductor element to convert the input RF voltage signal into a current signal. An inductor L_g is employed for input matching with the transconductor. The transconductor has inductive source degeneration, and it operates in the moderate inversion region [12]. The switching core of the mixer consists of devices M_2–M_5, and since this is a subharmonic mixer, a quadrature LO signal must be applied. While the single-balanced mixer configuration was chosen here to minimize the dc power consumption, the idea can be easily extended to a double-balanced arrangement.

The RF current signal first passes through the low impedance path created by the 1 pF RF current bypass capacitor C_{cr} that is connected between the drain of the M_1 and the sources of the PMOS device M_2–M_5. The mixer employs the complementary current-reuse design technique that alleviates the voltage headroom limitation imposed by the use of ultra-low supply voltage, compared with the conventional Gilbert cell design technique

Manuscript received July 24, 2011; revised October 29, 2011; accepted November 10, 2011. Date of publication January 12, 2012; date of current version February 03, 2012. This work was supported by a grant from the Natural Sciences and Engineering Research Council of Canada (NSERC).

The authors are with the Department of Electrical and Computer Engineering, Queen's University, Kingston, ON, Canada K7L 3N6 (e-mail: shan.he@queensu.ca; saavedra@queensu.ca).

Color versions of one or more of the figures in this paper are available online at http://ieeexplore.ieee.org.

Digital Object Identifier 10.1109/TMTT.2011.2178259

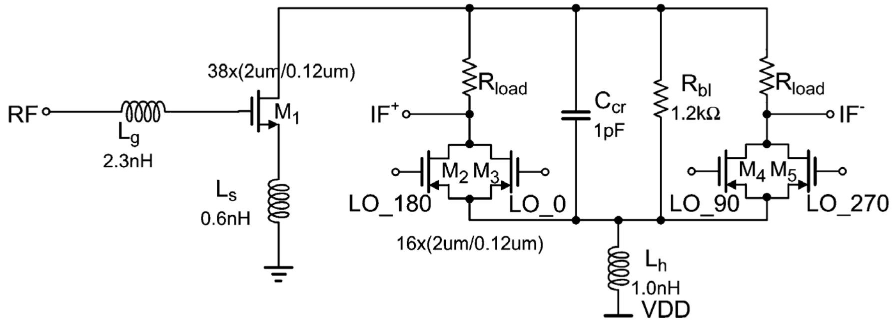

Fig. 1. Schematic of the proposed low-power/low-voltage $\times 2$ subharmonic mixer with device sizes annotated.

where a pair of stacked NMOS transistors are operated with high supply voltage [1], [3]. Inductor L_h is employed to alleviate the DC voltage headroom imposed by the ultra-low voltage condition and a high impedance path for the RF current. This technique provides the benefit of reusing the DC biasing current between the NMOS and the PMOS transistors when they are operated under the ultra-low supply voltage condition relative to the folded-switching design approach [13].

The RF current is then further processed by the commutating stage, which is composed of the PMOS transistors M_2 to M_5. Each of these PMOS switching transistors is connected to a quadrature phase of the LO signal. Together, they perform the action of $\times 2$ subharmonic mixing to the RF signal current, and then drive this $\times 2$ subharmonically down-converted differential signal to the loading resistors and the differential IF signal ports. The subharmonic mixing operation performed by the PMOS transistors M_2, M_3, M_4, and M_5 can be understood through a simplified analysis proposed in [8].

The mixer also uses the current-bleeding technique [4] by connecting a 1.2 kΩ DC current bleeding resistor, R_{bl}, between the source of the PMOS transistors and the drain of the NMOS transistor. Part of the DC biasing current flows through the current bleeding resistor to prevent excessive DC voltage drop across the loading resistors. As a result, higher conversion gain can be achieved by decreasing the resistance value of the bleeding resistors alone. Although by employing this current-bleeding technique, the increment of the mixer conversion gain is achieved at the expense of the linearity degradation; this however, does not pose a significant problem to our design since sufficiently high linearity is achieved with the inductive source degenerated transconductor.

B. Analysis of the Mixer's Distortion Behavior Using Volterra Series

The distortion generated in the RF transconductor stage is the determinant factor of the IP3 performance in an active Gilbert-type mixer [14]. CMOS transistors, when operated with a low supply voltage and low voltage bias, can enter into moderate inversion region. Device experiments with CMOS transistors have demonstrated significantly lower third order distortion content within a narrow gate bias region in the moderate inversion region [12]. In that narrow bias region, the transconductor has high linearity performance because the transistor drain current flow changes from exponentially dependent to slightly less than square-law-dependent on the gate-source biasing voltage. Somewhere in that region, a perfect square law relationship is achieved and the linearity performance is improved. This induces a natural peaking of the third-order input intercept point, IIP_3.

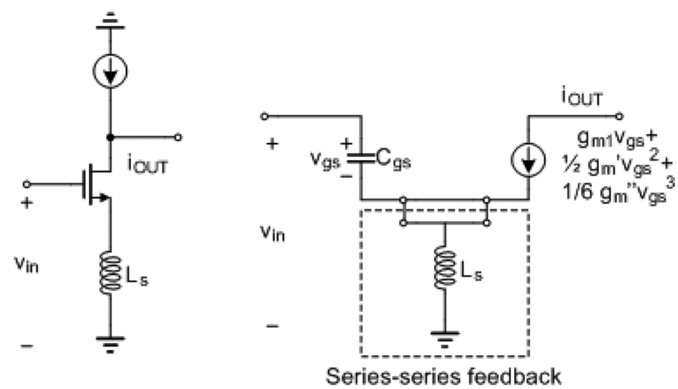

Fig. 2. Inductive source degenerated transconductor and its model.

Inductive source degeneration, shown in Fig. 2, employs series-series feedback that not only linearizes the transconductance of the transistor, but also provides a method to match the input impedance of the transconductor at a designed frequency [15]. The input impedance of the inductive source degenerated transconductor is described by

$$Z_{\mathrm{in}} = \frac{g_m L_s}{C_{gs}} + j\left(\omega L_s - \frac{1}{\omega C_{gs}}\right) \tag{1}$$

where g_m denotes the first-order transconductance of the transistor, C_{gs} denotes the effective gate-source capacitance of the transistor, and L_s denotes the source degeneration inductance. As the degeneration inductance increases, the improvement in the linearity is less pronounced and eventually there are no further benefits to source degeneration [16]. Nevertheless, a trade-off between the two can be reached to achieve a relatively high linearity. The effect of this trade-off on the inductive source degenerated transconductor is captured in detail by carrying out a Volterra series analysis based on the harmonic input method.

From Fig. 2, the current seen at the output of the source degenerated transconductor is defined by the following operation with respect to the input voltage, where each $\circ$ denotes the Volterra operand, ω's denote the dependent frequencies, G_1, G_2, and G_3 model the first, second, and third order transconductance of the transconductor, respectively:

$$i_o = G_1(\omega)\circ v_{\mathrm{in}} + G_2(\omega_1,\omega_2)\circ v_{\mathrm{in}}^2 + G_3(\omega_1,\omega_2,\omega_3)\circ v_{\mathrm{in}}^3. \tag{2}$$

Define the effective gate-source voltage recursively to the input voltage:

$$v_{gs} = A_1(\omega)\circ v_{\rm in} + A_2(\omega_1,\omega_2)\circ v_{\rm in}^2 + A_3(\omega_1,\omega_2,\omega_3)\circ v_{\rm in}^3. \quad (3)$$

Using the symbols g_m, g'_m, and g''_m to denote the transconductance of the transistor and its first and second derivatives, we can write that

$$\begin{aligned} i_o \cong\, & g_m A_1(\omega)\circ v_{\rm in} \\ & + \left[g_m A_2(\omega_1,\omega_2) + \frac{1}{2} g'_m A_1(\omega_1)A_1(\omega_2)\right]\circ v_{\rm in}^2 \\ & + \left[g_m A_3(\omega_1,\omega_2,\omega_3) + 2g'_m \overline{A_1(\omega_1)A_2(\omega_1,\omega_2)} \right. \\ & \left. + \frac{1}{3!} g''_m \overline{A_1(\omega_1)A_1(\omega_2)A_1(\omega_3)}\right]\circ v_{\rm in}^3. \end{aligned} \quad (4)$$

Working with (2)–(4) we can solve for the coefficients $A_1(\omega)$, $A_2(\omega_1,\omega_2)$ and $A_3(\omega_1,\omega_2,\omega_3)$. The results are shown below and a detailed derivation can be found in the Appendix:

$$\begin{aligned} A_1 =\, & 1/\left(V(\omega) + j\omega L_s g_m\right) \\ A_2 =\, & -j(\omega_1+\omega_2) \\ & \times L_s \frac{1}{2!} g'_m A_1(\omega_1)A_1(\omega_2)A_1(\omega_1+\omega_2) \\ A_3 =\, & -j(\omega_1+\omega_2+\omega_3)L_s A_1(\omega_1+\omega_2+\omega_3) \\ & \times \left[2g'_m \overline{A_1(\omega_1)A_2(\omega_1,\omega_2)} \right. \\ & \left. + \frac{1}{3!} g''_m \overline{A_1(\omega_1)A_1(\omega_2)A_1(\omega_3)}\right]. \end{aligned} \quad (5)$$

The function $V(\omega)$ in the expression for $A_1(\omega)$ above is given by

$$V(\omega) = (R_s + j\omega L_g)j\omega C_{gs} + 1 + (j\omega)^2 L_s C_{gs} + j\omega L_s g_m. \quad (6)$$

With further simplification of (4) and (5), the Volterra operators $G_1(\omega)$, $G_2(\omega_1,\omega_2)$ and $G_3(\omega_1,\omega_2,\omega_3)$ that describe the nonlinearity of the inductive source degenerated transconductor are found to be

$$\begin{aligned} G_1 =\, & g_m A_1(\omega) \\ G_2 =\, & \frac{1}{2} g'_m A_1(\omega_1)A_1(\omega_2)\left[1 - j(\omega_1+\omega_2)L_s g_m A_1(\omega_1+\omega_2)\right] \\ G_3 =\, & \left[2g'_m \overline{A_1(\omega_1)A_2(\omega_1,\omega_2)} + \frac{1}{3!} g''_m \overline{A_1(\omega_1)A_1(\omega_2)A_1(\omega_3)}\right] \\ & \times\left[1 - j(\omega_1+\omega_2+\omega_3)L_s g_m A_1(\omega_1+\omega_2+\omega_3)\right]. \end{aligned} \quad (7)$$

Now consider the in-band third-order intermodulation distortion with the desired signal at ω_s and the interferer at ω_i. Given that $2\omega_i - \omega_s \cong \omega_i \cong \omega_s$, we therefore have that

$$\begin{aligned} |G_3(\omega_i,\omega_i,-\omega_s)| =\, & |1 - j\omega L_s g_m A_1(\omega)|\,\left|A_1(\omega)^3\right| \\ & \times\left|\frac{1}{2} g''_m - \frac{2}{3} jL_s g'_m \left[2A_1(\Delta\omega)\Delta\omega + A_1(2\omega)2\omega\right]\right|. \end{aligned} \quad (8)$$

The linearity performance index of the transconductor, the third-order input intercept point [17], is described as

$$\mathrm{IIP}_3(2\omega_i - \omega_s) = \frac{1}{6}\frac{1}{R_s}\frac{|G_1(\omega_s)|}{|G_3(\omega_i,\omega_i,-\omega_s)|}. \quad (9)$$

Minimizing the magnitude of the third-order harmonic Volterra operator $G_3(\omega_i,\omega_i,-\omega_s)$ would naturally improve the linearity performance of the transconductor. Fig. 3 utilizes a vector diagram [17] to illustrate the interaction between the different components of $G_3(\omega_i,\omega_i,-\omega_s)$. From (8), the linearity performance of the transconductor, and its index IIP_3, are shown to be limited by two physical phenomenon, the third-order derivative of the transconductance g''_m and the harmonic feedback interaction between g'_m and L_s. Minimizing the former to 0 through the technique of optimum gate biasing without considering the additional constraints would maximize the linearity deterioration caused by the harmonic feedback interaction between g'_m and the series-series feedback inductor L_s.

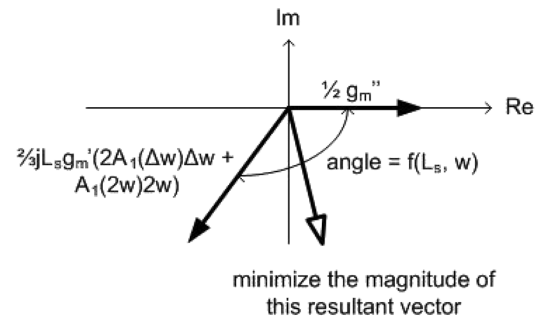

Fig. 3. Vector diagram for the components of $G_3(\omega_i,\omega_i,-\omega_s)$.

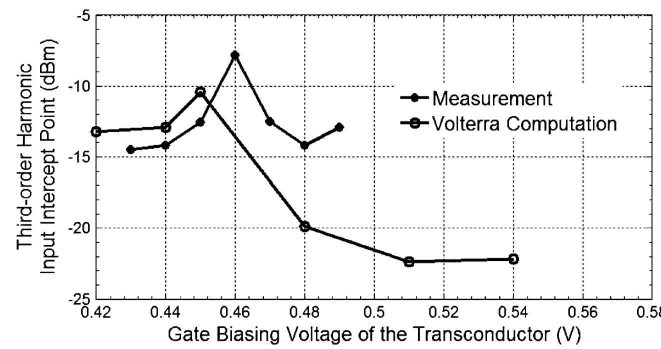

Fig. 4. Behavior of the third-order harmonic input intercept point of the transconductor computed with the Volterra series compared with the measured third-order harmonic input intercept point of the mixer.

Note that the first term of the last factor of $G_3(\omega_i,\omega_i,-\omega_s)$ in (8), $1/2g''_m$ is real, while the other term, $(2/3)jL_s g'_m[2A_1(\Delta\omega)\Delta\omega + A_1(2\omega)2\omega]$ is complex; since we are interested in minimizing the magnitude of $G_3(\omega_i,\omega_i,-\omega_s)$, a trade-off between these two phenomena that affect linearity is employed for best performance. The gate bias voltage of the transistor is varied to obtain different device transconductance values with its derivatives. Fig. 4 illustrates the behavior of the third-order harmonic input intercept point of the transconductor computed with the Volterra series using (7)–(9). We infer from Fig. 4 that the optimal gate biasing for the transconductor with inductive source degeneration is around 0.45 V.

To validate the Volterra analysis, circuit-level simulations using the SpectreRF simulator were also carried out. An extensive set of simulations were done to determine how the IIP_3 of the mixer changed as a function of both the gate bias voltage and the source degeneration inductance of transistor M_1 of the

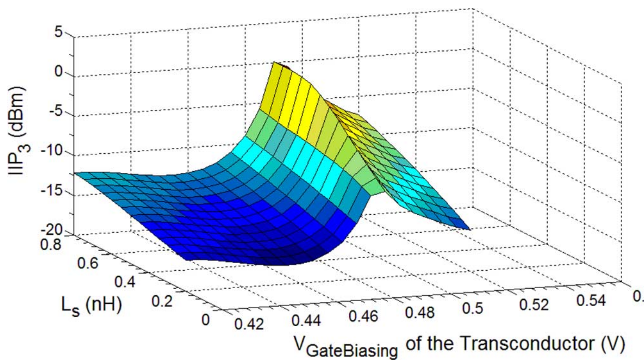

Fig. 5. Behavior of the third-order harmonic input intercept point of the mixer with varying transconductor gate biasing voltage and source degeneration inductance.

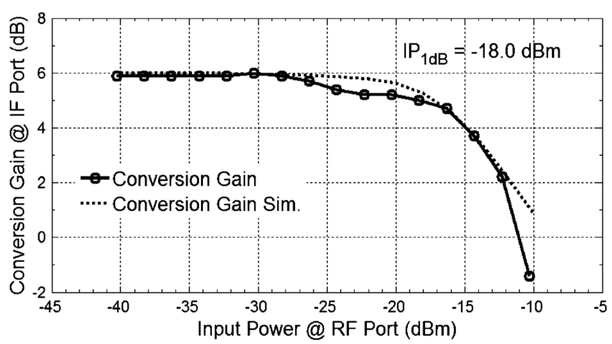

Fig. 6. Measured and simulated conversion gain of the mixer with the measured 1-dB compression point @ $f_{\mathrm{RF}} = 8.65$ GHz, $f_{\mathrm{LO}} = 4.3$ GHz.

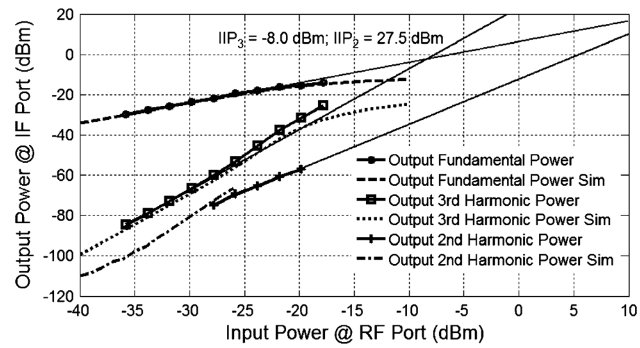

Fig. 7. Measured and simulated two-tone harmonic testing results of the mixer with an input frequency spacing of 20 MHz @ $f_{\mathrm{RF}} = 8.65$ GHz, $f_{\mathrm{LO}} = 4.3$ GHz.

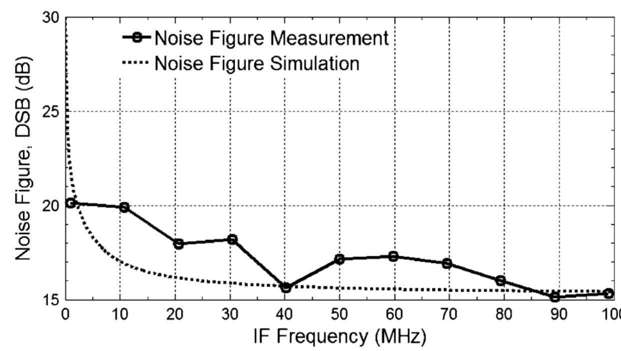

Fig. 8. Measured and simulated DSB noise figure of the mixer versus IF frequency.

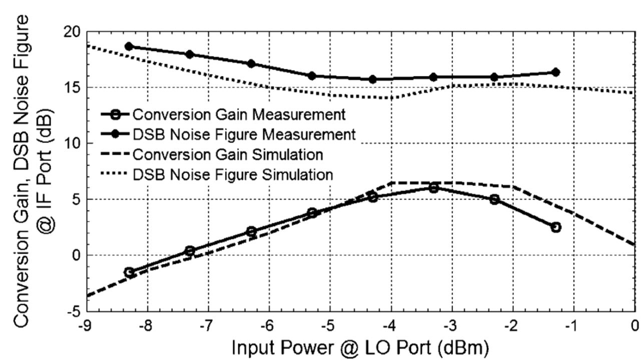

Fig. 9. Measured conversion gain and DSB noise figure of the mixer versus input LO power @ $f_{\mathrm{RF}} = 8.65$ GHz, $f_{\mathrm{LO}} = 4.3$ GHz.

RF stage. The results of the simulations are shown in Fig. 5. The graph shows that the highest IIP_3 values can be expected when the gate bias voltage is around 0.48 V, which is reasonably close to the value of 0.45 V obtained from the Volterra series results plotted in Fig. 4; while the optimal gate biasing inferred from the measurement result is somewhere in between these two values. It has been reported that the nonlinearity introduced by the switching stage would partially improve the linearity of the total mixer due to the interaction between the transconductor and the switching stage at high frequency [18], which explains the values of the third-order harmonic input intercept points of the transconductor based on the Volterra computation being lower in magnitude.

III. Experimental Results

To demonstrate the validity of the proposed circuit design, the single-balanced $\times 2$ subharmonic ultra-low-voltage down-conversion mixer is designed and fabricated using a standard 130 nm CMOS process from IBM. An on-chip probed measurement is performed to validate the design. All off-chip losses from the cables and the power combiners were calibrated at their operation frequency and de-embedded in the measurement results. To facilitate the testing setup, a RC-CR 90° phase-shifter is designed on-chip to generate the required quadrature LO signals.

With a RF input frequency of 8.65 GHz and a LO frequency of 4.3 GHz, the IF output frequency is at 50 MHz for this single-balanced $\times 2$ subharmonic down-conversion mixer. Fig. 6 illustrates the 1-dB input compression point with input LO power of -3.3 dBm. This set of measurements indicates the $P_{\mathrm{in-1dB}}$ compression point to be -18.0 dBm. Fig. 7 illustrates the linearity measurements of the mixer obtained from a two-tone harmonic testing with a frequency spacing of 20 MHz. The third-order input intercept point IIP_3 is measured to be -8.0 dBm. The second-order input intercept point IIP_2 is measured to be 27.5 dBm. Furthermore, a minimum double-side-band (DSB) noise figure of 15.9 dB is obtained via a noise figure measurement, as shown in Fig. 8.

Fig. 9 illustrates the measured down-conversion power gain and DSB noise figure at the IF port as a function of the input LO power at the LO port. This set of measurements indicates that the mixer has a peak conversion gain of 6.0 dB and DSB noise figure of 15.9 dB with an input LO power of -3.3 dBm. This

TABLE I
PERFORMANCE SUMMARY AND COMPARISON WITH SILICON-BASED ACTIVE MIXERS

		This Work	[6]	[5]	[3]†	[7]	[19]
CMOS Node		130 nm	180 nm	180 nm	180 nm	180 nm	130 nm
RF Frequency	(GHz)	8.65	5.25	0.9	5.2	2.4	2.2
LO Frequency	(GHz)	4.3	2.62	0.45	5.1	1.2	1.1
Supply Voltage	(V)	0.6	0.9	1.8	0.6	1.8	1.2
DC Power	(mW)	0.6	5.0	1.4	0.8	4.5	7.2
LO Power	(dBm)	-3.3	5.5	5.0	-2.0	-10.0	-18.0
Conversion Gain	(dB)	6.0	8.3	9.17	3.2	26.0	4.5
$P_{1dB,in}$	(dBm)	-18.0	-15.0	-14.5	-15.0	-	-
IIP_3	(dBm)	-8.0	0.0	-5.0	-8.0	-10.0	0.0
IIP_2	(dBm)	27.5	31.2	-	-	-	35.0
DSB Noise Figure	(dB)	15.9	24.5	30.5	14.0	9.0	11.0
Input Matching?		Yes	No	Yes	Yes	Yes	Yes

† Fundamental mixer

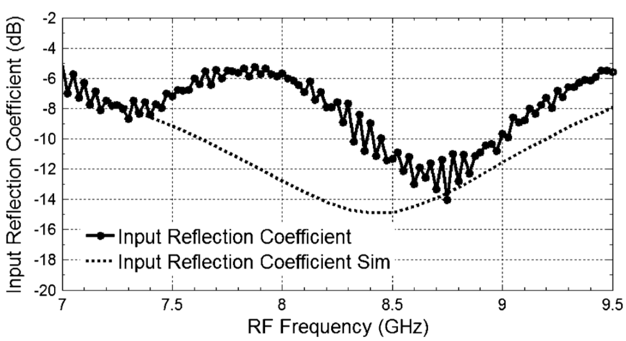

Fig. 10. Measured and simulated input reflection coefficient of the mixer.

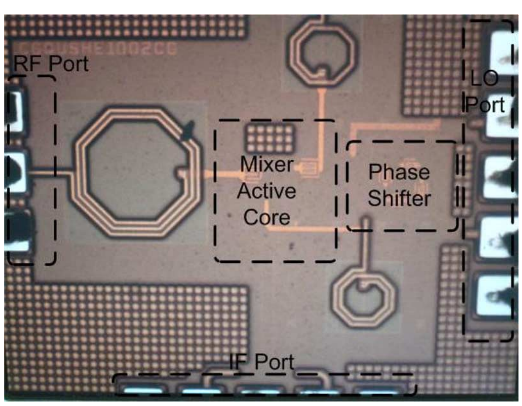

Fig. 11. Chip microphotograph.

set of measurements further confirms the feasibility of the designed mixer in a high frequency RF system with the ultra-low supply voltage of 0.6 V since the input LO power is theoretically bounded by -0.5 dBm, i.e. a maximum LO voltage swing of 0.6 V. Furthermore, a 2× LO leakage isolation is measured to be around 31.2 dB.

Fig. 10 shows the reflection coefficient of the mixer at the RF port. The return loss is around 12 dB at the design frequency of 8.6 GHz. The additional inductor L_g is designed to cancel out the negative imaginary part of the input impedance of the transconductor at around 8.5 GHz.

The circuit core occupies of approximately 0.4 mm^2, and a photograph of the fabricated chip is shown in Fig. 11. The mixer circuit draws 0.6 mW of dc power from a 0.6 V supply.

A performance summary of the mixer plus a comparison to other silicon-based active mixers is presented in Table I. It is seen that the mixer in this paper achieves the lowest dc power consumption and has the highest RF operating frequency. In addition, this mixer uses the lowest dc power supply voltage level in the subharmonic category.

IV. CONCLUSIONS

An ultra-low-voltage low-power single-balanced ×2 subharmonic down-conversion mixer was designed and measured. The linearity analysis for the inductive source degenerated transconductor of the mixer is provided using Volterra series. This analysis provides a guideline for designing the inductive source degenerated transconductor with high linearity at the high RF frequency of 8.6 GHz. We then proceed to propose the ultra-low-voltage low-power single-balanced ×2 subharmonic mixer circuit, which performs a ×2 subharmonic down-conversion mixing. We obtained a conversion gain of 6.0 dB and an IIP_3 of -8.0 dBm at the RF frequency of 8.6 GHz while consuming 0.6 mW of DC power with the supply voltage of 0.6 V.

APPENDIX
DERIVATION OF THE VOLTERRA OPERATORS FOR THE INDUCTIVE SOURCE DEGENERATED TRANSCONDUCTOR

The current seen at the output of the source degenerated transconductor is first expressed as

$$i_o = G_1(\omega)\circ v_{\text{in}} + G_2(\omega_1,\omega_2)\circ v_{\text{in}}^2 + G_3(\omega_1,\omega_2,\omega_3)\circ v_{\text{in}}^3. \quad (10)$$

Substituting the defined relationship between the effective gate-source voltage and the input voltage

$$v_{gs} = A_1(\omega)\circ v_{\text{in}} + A_2(\omega_1,\omega_2)\circ v_{\text{in}}^2 + A_3(\omega_1,\omega_2,\omega_3)\circ v_{\text{in}}^3 \quad (11)$$

to the device equation relating the device transconductance (with its derivatives) and the effective gate-source voltage

$$i_o = g_m v_{gs} + \left(\frac{1}{2!}g'_m\right) v_{gs}^2 + \left(\frac{1}{3!}g''_m\right) v_{gs}^3. \quad (12)$$

Taking terms up to the third order, the nonlinear transfer function of the output current is

$$\begin{aligned} i_o \cong\, & g_m A_1(\omega) \circ v_{\text{in}} \\ & + \left[g_m A_2(\omega_1,\omega_2) + \frac{1}{2}g'_m A_1(\omega_1)A_1(\omega_2)\right] \circ v_{\text{in}}^2 \\ & + \Big[g_m A_3(\omega_1,\omega_2,\omega_3) + 2g'_m \overline{A_1(\omega_1)A_2(\omega_1,\omega_2)} \\ & \qquad + \frac{1}{3!}g''_m \overline{A_1(\omega_1)A_1(\omega_2)A_1(\omega_3)}\Big] \circ v_{\text{in}}^3. \end{aligned} \quad (13)$$

With

$$v_{\text{in}} = v_{gs}\left[(R_s + sL_g)sC_{gs} + 1 + s^2 L_s C_{gs} + sL_s g_m\right] + sL_s io \quad (14)$$

where R_s is the RF input port source impedance,

$$\begin{aligned} v_{\text{in}} = & \left[A_1(\omega)\circ v_{\text{in}} + A_2(\omega_1,\omega_2)\circ v_{\text{in}}^2 + A_3(\omega_1,\omega_2,\omega_3)\circ v_{\text{in}}^3\right] \\ & \times \left[(R_s + sL_g)sC_{gs} + 1 + s^2 L_s C_{gs} + sL_s g_m\right] + sL_s \\ & \times \Big\{g_m A_1(\omega)\circ v_{\text{in}} \\ & \quad + \left[g_m A_2(\omega_1,\omega_2) + \left(\frac{1}{2}g'_m\right) A_1(\omega_1)A_1(\omega_2)\right]\circ v_{\text{in}}^2 \\ & \quad + \Big[g_m A_3(\omega_1,\omega_2,\omega_3) + 2g'_m \overline{A_1(\omega_1)A_2(\omega_1,\omega_2)} \\ & \qquad + \frac{1}{3!}g''_m \overline{A_1(\omega_1)A_1(\omega_2)A_1(\omega_3)}\Big]\circ v_{\text{in}}^3\Big\}. \end{aligned} \quad (15)$$

Collecting the first-order terms of the previous equation,

$$1 = A_1(\omega)V(\omega) + j\omega L_s g_m A_1(\omega) \quad (16)$$

where

$$V(\omega) = (R_s + j\omega L_g)j\omega C_{gs} + 1 + (j\omega)^2 L_s C_{gs} + j\omega L_s g_m. \quad (17)$$

$A_1(\omega)$ is solved recursively as

$$A_1(\omega) = \frac{1}{V(\omega) + j\omega L_s g_m}. \quad (18)$$

Collecting the second-order terms in a very similar fashion,

$$\begin{aligned} 0 = & A_2(\omega_1,\omega_2)V(\omega_1+\omega_2) + j(\omega_1+\omega_2) \\ & \times L_s\left[g_m A_2(\omega_1,\omega_2) + \left(\frac{1}{2!}g'_m\right) A_1(\omega_1)A_1(\omega_2)\right], \end{aligned} \quad (19)$$

$$\begin{aligned} A_2(\omega_1,\omega_2) &= \frac{-j(\omega_1+\omega_2)L_s \frac{1}{2!}g'_m A_1(\omega_1)A_1(\omega_2)}{V(\omega_1+\omega_2) + j(\omega_1+\omega_2)L_s g_m} \\ &= -j(\omega_1+\omega_2)L_s \frac{1}{2!}g'_m A_1(\omega_1)A_1(\omega_2)A_1(\omega_1+\omega_2). \end{aligned} \quad (20)$$

Similarly,

$$\begin{aligned} 0 = & A_3(\omega_1,\omega_2,\omega_3)V(\omega_1+\omega_2+\omega_3) \\ & + j(\omega_1+\omega_2+\omega_3)L_s\Big[g_m A_3(\omega_1,\omega_2,\omega_3) \\ & \qquad + 2g'_m \overline{A_1(\omega_1)A_2(\omega_1,\omega_2)} \\ & \qquad + \frac{1}{3!}g''_m \overline{A_1(\omega_1)A_1(\omega_2)A_1(\omega_3)}\Big]. \end{aligned} \quad (21)$$

Collecting the third-order terms, $A_3(\omega_1,\omega_2,\omega_3)$ is therefore solved recursively as

$$\begin{aligned} A_3(\omega_1,\omega_2,\omega_3) = & -j(\omega_1+\omega_2+\omega_3)L_s A_1(\omega_1+\omega_2+\omega_3) \\ & \times \left[2g'_m \overline{A_1(\omega_1)A_2(\omega_1,\omega_2)} + \frac{1}{3!}g''_m \overline{A_1(\omega_1)A_1(\omega_2)A_1(\omega_3)}\right]. \end{aligned} \quad (22)$$

Substitute A_1, A_2 and A_3 back to the nonlinear transfer function in (15),

$$\begin{aligned} G_1 = & g_m A_1(\omega) \\ G_2 = & -j(\omega_1+\omega_2)L_s g_m \frac{1}{2}g'_m \\ & \times A_1(\omega_1)A_1(\omega_2)A_1(\omega_1+\omega_2) + \frac{1}{2}g'_m A_1(\omega_1)A_1(\omega_2) \\ = & \frac{1}{2}g'_m A_1(\omega_1)A_1(\omega_2)\left[1 - j(\omega_1+\omega_2)L_s g_m A_1(\omega_1+\omega_2)\right] \\ G_3 = & \left[2g'_m \overline{A_1(\omega_1)A_2(\omega_1,\omega_2)} + \frac{1}{3!}g''_m \overline{A_1(\omega_1)A_1(\omega_2)A_1(\omega_3)}\right] \\ & \times \left[1 - j(\omega_1+\omega_2+\omega_3)L_s g_m A_1(\omega_1+\omega_2+\omega_3)\right]. \end{aligned} \quad (23)$$

Consider in-band third-order intermodulation distortion with the desired signal at ω_s and the interferer at ω_i, the in-band third-order intermodulation distortion is then located at the frequency where $2\omega_i - \omega_s \cong \omega_i \cong \omega_s$.

$\overline{A_1(\omega_1)A_2(\omega_1,\omega_2)}$ is therefore can be approximated at the in-band third-order intermodulation distortion frequency as

$$\begin{aligned} \overline{A_1 A_2} = & \frac{1}{3}\Big[A_1(\omega_i)(-j)\Delta\omega L_s \frac{1}{2}g'_m A_1(\omega)A_1(\omega)A_1(\Delta\omega) \\ & \quad + A_1(\omega_i)(-j)\Delta\omega L_s \frac{1}{2}g'_m A_1(\omega)A_1(\omega)A_1(\Delta\omega) \\ & \quad + A_1(-\omega_s)(-j)2\omega L_s \frac{1}{2}g'_m A_1(\omega)A_1(\omega)A_1(2\omega)\Big] \\ \cong & -jL_s \frac{1}{6}g'_m A_1(\omega)\left|A_1(\omega)\right|^2 \\ & \times \left[2A_1(\Delta\omega)\Delta\omega + A_1(2\omega)2\omega\right]. \end{aligned} \quad (24)$$

Furthermore, at the in-band third-order distortion frequency,

$$\begin{aligned} & |G_3(\omega_i,\omega_i,\omega_{-s})| \\ & \quad = |1 - j\omega L_s g_m A_1(\omega)|\left|A_1(\omega)^2\right| \\ & \qquad \times \Big|-j\frac{2}{3}g'_m L_s A_1(\omega)\left[2\Delta\omega A_1(\Delta\omega)\right. \\ & \qquad\qquad \left. + 2\omega A_1(2\omega)\right] + \frac{1}{2}g''_m A_1(\omega)\Big| \\ & \quad = |1 - j\omega L_s g_m A_1(\omega)|\left|A_1(\omega)^3\right| \\ & \qquad \times \left|\frac{1}{2}g''_m - \frac{2}{3}jL_s g'_m\left[2A_1(\Delta\omega)\Delta\omega + A_1(2\omega)2\omega\right]\right|. \end{aligned} \quad (25)$$

ACKNOWLEDGMENT

The authors would like to thank CMC Microsystems, Kingston, Ontario, Canada, for their support and access to IC fabrication services.

REFERENCES

[1] L.-H. Lu and H.-S. Chen, "Lower the voltage for CMOS RFIC," *IEEE Microw. Mag.*, vol. 11, no. 1, pp. 70–77, 2010.
[2] P. Kinget, "Designing analog and RF circuits in nanoscale CMOS technologies: Scale the supply, reduce the area and use digital gates," in *Proc. IEEE Int. Conf. Microwaves, Communications, Antennas and Electronics Systems*, 2009, p. 1.
[3] H.-H. Hsieh and L.-H. Lu, "Design of ultra-low-voltage RF frontends with complementary current-reused architectures," *IEEE Trans. Microw. Theory Tech.*, vol. 55, no. 7, pp. 1445–1458, 2007.
[4] S.-G. Lee and J.-K. Choi, "Current-reuse bleeding mixer," *Electron. Lett.*, vol. 36, no. 8, pp. 696–697, Apr. 2000.
[5] S.-Y. Lee, M.-F. Huang, and C. Kuo, "Analysis and implementation of a CMOS even harmonic mixer with current reuse for heterodyne/direct conversion receivers," *IEEE Trans. Circuits Syst. I: Reg. Papers*, vol. 52, no. 9, pp. 1741–1751, 2005.
[6] M.-F. Huang, C. Kuo, and S.-Y. Lee, "A 5.25-GHz CMOS folded-cascode even-harmonic mixer for low-voltage applications," *IEEE Trans. Microw. Theory Tech.*, vol. 54, no. 2, pp. 660–669, 2006.
[7] T. Hui Teo and W. G. Yeoh, "Low-power short-range radio CMOS subharmonic RF front-end using CG-CS LNA," *IEEE Trans. Circuits Syst. II: Expr. Briefs*, vol. 55, no. 7, pp. 658–662, 2008.
[8] B. Jackson and C. Saavedra, "A CMOS Ku-band 4× subharmonic mixer," *IEEE J. Solid-State Circuits*, vol. 43, no. 6, pp. 1351–1359, Jun. 2008.
[9] K. Nimmagadda and G. Rebeiz, "A 1.9 GHz double-balanced subharmonic mixer for direct conversion receivers," in *IEEE Radio Frequency Integrated Circuits (RFIC) Symp. Dig.*, 2001, pp. 253–256.
[10] K. Maeda, E. Taniguchi, M. Ono, N. Suematsu, and T. Takagi, "A 2 GHz band even harmonic type SI-MMIC active balanced CECCTP mixer," in *Eur. Microwave Conf.*, Sep. 2001, pp. 1–4.
[11] R. Svitek and S. Raman, "DC offsets in direct-conversion receivers: Characterization and implications," *IEEE Microw. Mag.*, vol. 6, no. 3, pp. 76–86, 2005.
[12] V. Aparin, G. Brown, and L. Larson, "Linearization of CMOS LNA's via optimum gate biasing," in *Proc. IEEE Int. Symp. Circuits and Systems (ISCAS)*, May 2004, vol. 4, pp. IV-748–IV-751.
[13] V. Vidojkovic, J. van der Tang, A. Leeuwenburgh, and A. van Roermund, "A low-voltage folded-switching mixer in 0.18-μm CMOS," *IEEE J. Solid-State Circuits*, vol. 40, no. 6, pp. 1259–1264, Jun. 2005.
[14] B. Gilbert, "The micromixer: A highly linear variant of the Gilbert mixer using a bisymmetric class-AB input stage," *IEEE J. Solid-State Circuits*, vol. 32, no. 9, pp. 1412–1423, Sep. 1997.
[15] T.-K. Nguyen, C.-H. Kim, G.-J. Ihm, M.-S. Yang, and S.-G. Lee, "CMOS low-noise amplifier design optimization techniques," *IEEE Trans. Microw. Theory Tech.*, vol. 52, no. 5, pp. 1433–1442, May 2004.
[16] B. Toole, C. Plett, and M. Cloutier, "RF circuit implications of moderate inversion enhanced linear region in MOSFETs," *IEEE Trans. Circuits Syst. I: Reg. Papers*, vol. 51, no. 2, pp. 319–328, 2004.
[17] V. Aparin and L. Larson, "Modified derivative superposition method for linearizing FET low-noise amplifiers," *IEEE Trans. Microw. Theory Tech.*, vol. 53, no. 2, pp. 571–581, 2005.
[18] M. Terrovitis and R. Meyer, "Intermodulation distortion in current-commutating CMOS mixers," *IEEE J. Solid-State Circuits*, vol. 35, no. 10, pp. 1461–1473, Oct. 2000.
[19] H. Jen, S. Rose, and R. Meyer, "A 2.2 GHz sub-harmonic mixer for direct conversion receivers in 0.13μm CMOS," in *IEEE Int. Solid-State Circuits Conf. Dig. Tech. Papers*, Feb. 2006, pp. 1840–1849.

Shan He received the B.Sc. (Hon.) degree in electrical engineering from the University of Toronto, Toronto, ON, Canada, in 2008, and the M.A.Sc. degree at Queen's University, Kingston, ON, Canada, in 2011.

He is now with Marvell Semiconductor. His research interests are in the field of radio-frequency integrated circuits such as mixers, amplifiers, and passive microwave components. His current research is focused on low-voltage radio-frequency front-end circuits.

Mr. He was a recipient of an NSERC Postgraduate Scholarship and an Ontario Graduate Scholarship.

Carlos E. Saavedra (S'92–M'98–SM'05) received the Ph.D. degree in electrical engineering from Cornell University, Ithaca, NY, in 1998.

From 1998 to 2000, he was with Millitech Corporation, South Deerfield, MA. Since 2000, he has been with Queen's University, Kingston, ON, Canada, where he is now an Associate Professor. He served as Graduate Chair for the Department of Electrical and Computer Engineering from 2007 to 2010.

Dr. Saavedra is the Chair of the IEEE MTT-S Technical Coordinating Committee 22: Signal Generation and Frequency Conversion. He is a member of the 2012 IEEE International Microwave Symposium Steering Committee and he served on the Technical Program Committee of the IEEE RFIC Symposium from 2008 to 2011. He is a reviewer for several journals, including the IEEE TRANSACTIONS ON MICROWAVE THEORY AND TECHNIQUES, the IEEE JOURNAL OF SOLID-STATE CIRCUITS, the *IEEE Microwave and Wireless Components Letters*, and the IEEE TRANSACTIONS ON CIRCUITS AND SYSTEMS PARTS I AND II. He is a registered Professional Engineer (P. Eng.) in the province of Ontario, Canada.